IEEE Photonics Journal
An IEEE Photonics Society Publication

RF Up-Conversion and Waveform Generation Using a Frequency-Shifting Amplifying Fiber Loop, Application to Doppler Velocimetry

Volume 09, Number 6, December 2017

Hongzhi Yang
Marc Brunel
Haiyang Zhang
Marc Vallet
Changming Zhao
Suhui Yang

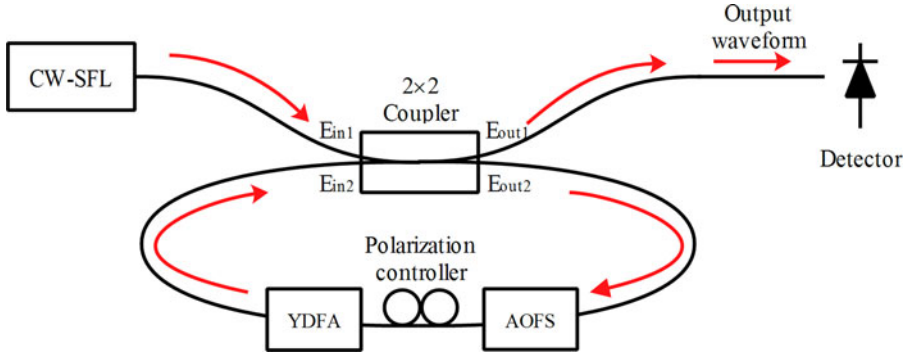

DOI: 10.1109/JPHOT.2017.2775617
1943-0655

RF Up-Conversion and Waveform Generation Using a Frequency-Shifting Amplifying Fiber Loop, Application to Doppler Velocimetry

Hongzhi Yang,[1] **Marc Brunel**,[2] **Haiyang Zhang**,[1] **Marc Vallet**,[2] **Changming Zhao**,[1] **and Suhui Yang** [1]

[1]School of Optoelectronics, Beijing Institute of Technology, Beijing 100081, China
[2]Institut FOTON/DOP, Université de Rennes 1 – CNRS UMR 6082, Rennes 35042, France

DOI:10.1109/JPHOT.2017.2775617

Manuscript received October 11, 2017; revised October 31, 2017; accepted November 16, 2017. Date of publication November 20, 2017; date of current version November 30, 2017. Corresponding author: Haiyang Zhang (e-mail: ocean@bit.edu.cn).

Abstract: We investigate the radio-frequency (RF) up-conversion and waveform generation properties of an optical fiber loop including a frequency shifter and an amplifier. By seeding the loop with a single-frequency continuous-wave laser, one can develop a wide optically carried RF comb, whose spectral extension is governed by the loop net gain. In addition, by choosing the fiber loop length and the RF shifting frequency, arbitrary waveforms can be generated. We present an analytical interference model that includes the time delay, the frequency shift, and the gain. Experiments are conducted with 1.06-μm fiber-optic components. Using a 200-MHz acousto-optic frequency shifter, we find a 19-fold up-conversion up to 3.8 GHz with a typical in-loop gain of 3. Various waveforms including bright and dark pulses, square- or triangle shaped are achieved by properly adjusting the loop length and the frequency shift. A good agreement between experimental and theoretical results is obtained. The fully fibered microwave-photonic source is applied to a laboratory Doppler velocimetry demonstration. The gain in sensitivity obtained with the up-converted signal is readily observed.

Index Terms: Radio frequency photonics, fiber optics links and subsystems.

1. Introduction

Lidar-radar is a powerful technique for applications involving remote sensing. The method is based on the use of an optically carried RF signal in order to benefit from both the directivity of the optical beam (lidar), and the accuracy of RF signal processing (radar) [1]–[4]. Compared with single-optical-frequency lidars, coherent RF-modulated lidar-radars are insensitive to atmospheric turbulence [5] and can overcome the speckle noise induced by target's roughness [5]–[7]. However, lidar-radar velocimetry still has to face the challenge of ultra-low Doppler frequency shift (in the mHz-Hz range), whose impact can be reduced by enhancing the modulation frequency. In this context, high-frequency RF modulation of laser beams can be obtained by the use of offset-injection locked laser diodes [3], mode-locked lasers [8], [9] or by multipass frequency-shifting external cavity coupled to a single-frequency laser [10]. Here we aim at extending the technique developed previously with a free-space pulsed laser [10] to an efficient fully fibered ring interferometer seeded by a single-frequency laser.

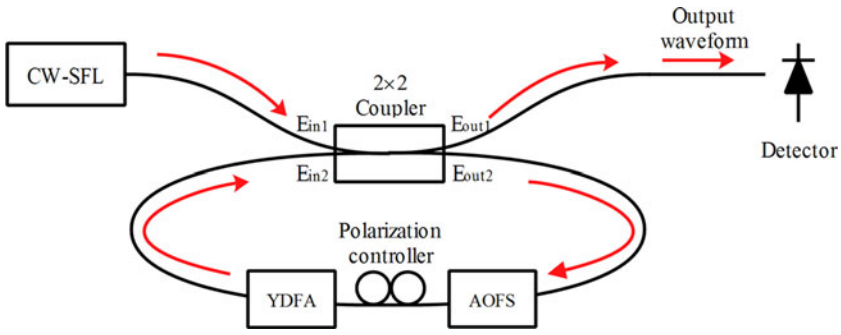

Fig. 1. Principle of the fiber frequency-shifting amplifier loop: SFL: single-frequency laser, AOFS: fiber acousto-optic frequency-shifter. YDFA: ytterbium-doped fiber amplifier.

Ring interferometers containing both an amplifier and a frequency-shifter have been proposed in different contexts, either for enhancing the performance of self-heterodyne laser linewidth measurements, or for frequency-shifted feedback (FSF) lasing and mode-locked operation. In the first application, the recirculating loop is as long as possible to overcome the laser linewidth to be measured [11], and the insertion of an amplifier permits to reduce the impact of losses over many round-trips [12], [13]. In the FSF laser case, pulsed regimes are readily observed [14], [15]. When the frequency shift is tuned to a fraction of the cavity free-spectral range, periodic pulse trains can be generated leading to a "Talbot laser" [16]. Similar set-ups were recently shown to provide high data-rates in radio-over-fiber communications [17], real-time Fourier transformation of optical signals [18], or rapid wavelength scanning [19].

The aim of this article is to show that the recirculating frequency-shifting ring interferometer is a convenient method for radio-frequency up-conversion and waveform generation, and that it can be readily implemented as lidar-radar source. In our work, we focus on (i) loop lengths shorter than the seed coherence length in order to provide high-purity RF harmonic beats, and (ii) seeded sub-threshold operation in order to control the RF phase and amplitudes of the recirculating components. We provide a theoretical model to derive a time-delayed interference equation to obtain the output intensity of the loop, and we compare it with an all-fibered experiment based on 1 μm fiber-optics components. In Section 2, we describe the experimental setup and introduce the time-delayed interference equation. Section 3 presents the simulation and experimental results. Frequency up-conversion is studied with respect to the gain parameter. Then we investigate the different waveforms produced when varying the loop length or the frequency shift. Section 4 is devoted to a direct application of this RF up-conversion method, namely a Doppler velocimetry experiment. We show that the 15-fold enhancement in the beat frequency yields improved velocity resolution especially at low target speeds. Finally, conclusions are given in Section 5.

2. System Description

We consider an optical fiber ring interferometer as depicted in Fig. 1. A continuous-wave single-frequency fiber laser is connected to the input port 1 of a 2 $\times$ 2 fiber coupler. The output port 2 is sent through a frequency shifter followed by an amplifier back to the input port 2 of the coupler. Hence we find at the output port 1 the interference of the input wave with the summation of time-delayed, frequency-shifted, recirculating loop waves.

In order to predict the output waveform, we derive a time-delayed scalar interference equation. We write t_{ij} the transmission coefficients of the coupler. Given E_{inj} the input electric field components at inputs *i,j* of the coupler, the output field components E_{outi} can be written as follows:

$$\begin{bmatrix} E_{out1} \\ E_{out2} \end{bmatrix} = \begin{bmatrix} t_{11} & t_{12} \\ t_{21} & t_{22} \end{bmatrix} \begin{bmatrix} E_{in1} \\ E_{in2} \end{bmatrix} \tag{1}$$

In the case of an ideal coupler, that is a lossless and symmetrical coupler, the matrix [t] is unitary and can be written [20]

$$[t] = \begin{bmatrix} t_{11} & t_{12} \\ -t_{12}^{*} & t_{11}^{*} \end{bmatrix} \text{ with } |t_{11}|^2 + |t_{12}|^2 = 1 \tag{2}$$

Inside the loop, the AOFS is driven by a synthesizer at frequency f_{AO}. The propagation time for one round-trip in the loop is τ. We define γ as the complex number that takes into account the transmissions of the loop components, as well as the associated phase shifts. If η and G are the intensity transmission of the AOFS and the intensity gain of the YDFA, respectively, then $\gamma = \sqrt{\eta G}\, e^{j\varphi}$, where φ is a constant phase shift that can be set to 0 by changing the origin of time. E_{out2} can be deduced from E_{in1} using

$$E_{out2}(t) = t_{21} \sum_{p=0}^{\infty} (t_{22}\gamma)^p E_{in1}(t - p\tau)\, e^{j2\pi f_{AO} p (t-\tau)}\, e^{-i\pi f_{AO} p^2 \tau}. \tag{3}$$

The experimentally accessible and useful output is the output port 1. At this port, we find

$$\begin{aligned} E_{out1}(t) &= t_{11} E_{in1}(t) + t_{12} E_{in2}(t) \\ &= t_{11} E_{in1}(t) + t_{12}\gamma E_{out2}(t-\tau) e^{j2\pi f_{AO}(t-\tau)} \\ &= t_{11} E_{in1}(t) + t_{12}\gamma t_{21} \sum_{p=1}^{\infty} (t_{22}\gamma)^{(p-1)} E_{in1}(t - p\tau) e^{-i\pi f_{AO} p\tau} e^{j2\pi f_{AO} p t} e^{-i\pi f_{AO} p^2 \tau}. \end{aligned} \tag{4}$$

If the input field at port 1 is a monochromatic field with infinite coherence time and optical power P_{in}, then the useful output power reads

$$P_{out}(t) = \left| t_{11} + t_{12}\gamma t_{21} \sum_{p=1}^{\infty} (t_{22}\gamma)^{(p-1)} e^{-i\pi f_{AO} p\tau} e^{j2\pi f_{AO} p t} e^{-i\pi f_{AO} p^2 \tau} \right|^2 P_{in} \tag{5}$$

Finally, the output power can be written as a sum of RF-harmonics P_n

$$P_{out}(t) = P_0 + \sum_{n=1}^{\infty} \left[P_n e^{j2\pi n f_{AO} t} + cc \right] \tag{6}$$

For an ideal coupler, a straightforward calculation using (2) yields the following expression for the nth harmonic power:

$$|P_n| = (\Gamma T_{11})^{n/2} T_{12} \sqrt{\frac{(1-\Gamma)^2 + 4\Gamma \sin^2(n\pi f_{AO}\tau)}{(1-\Gamma T_{11})^2 + 4\Gamma T_{11} \sin^2(n\pi f_{AO}\tau)}} \tag{7}$$

with $\Gamma = |\gamma^2|$ and $T_{ij} = |t_{ij}|^2$. In agreement with previous descriptions of the ring interferometer, (5) and (7) show the influence of the relevant experimental parameters that will be used in the following: the delay time τ, the frequency shift f_{AO}, and the loop transmission coefficient γ.

Our experiments are performed with a monomode fiber laser, which typically delivers 50 mW at 1064 nm. Its linewidth is about 2 kHz. From the measured values of the intensity transmission coefficients, the coupling matrix is set to $[t] = \begin{bmatrix} 0.60 & 0.59j \\ 0.54j & 0.60 \end{bmatrix}$. The nominal frequency shift is $f_{AO} =$ 200 MHz, but it can be adjusted between 195 MHz and 205 MHz. The maximal diffraction efficiency is measured to be $\eta = 0.41$. G is the less well-known parameter because of the saturation effects when the loop is closed. However, taking insertion losses into account, we will consider gains of typically less than 5 in order to avoid loop oscillations, that is $G < 1/(T_{22}\Gamma)$. The optical length $n_g L$ (with n_g the group index) of the loop is in the range of 20 m, leading to a delay time τ of the order of 10^{-7} s, and can be simply adjusted by discrete amounts by adding short pieces of fiber. The coherence time of the seed laser is thus considerably higher than the loop delay time, as it is

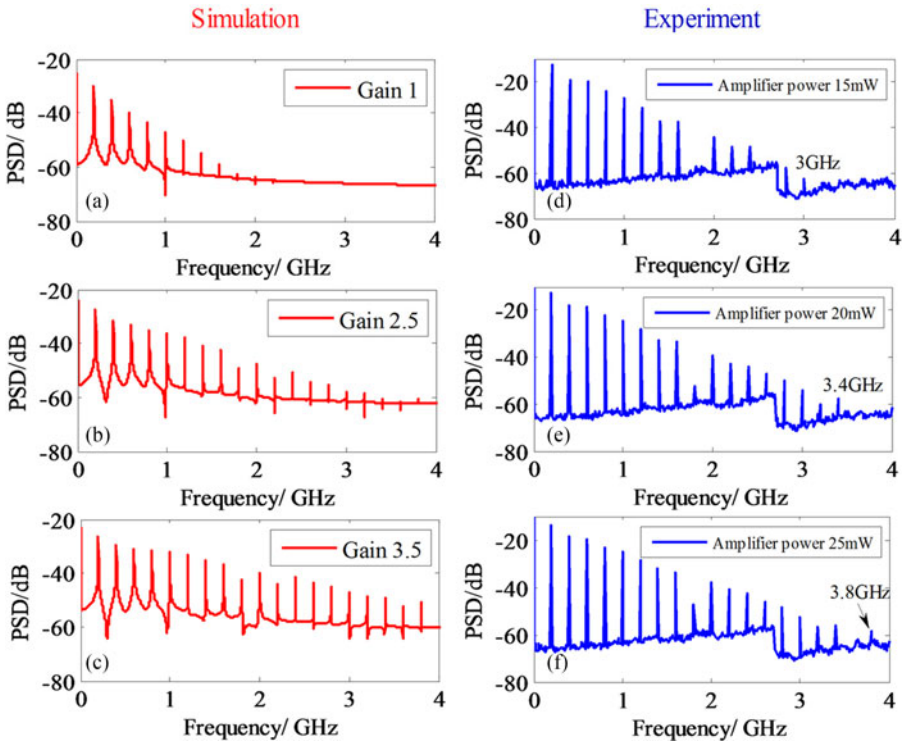

Fig. 2. Influence of the loop net gain on the power spectral density (PSD) of the beat note. Simulations (in red): (a) G = 1, (b) G = 2.5, and (c) G = 3.5. Experiments (in blue), when amplifier power is set to (d) 15 mW, (e) 20 mW, and (f) 25 mW.

verified in the following experiments. Experimentally we use an amplifier that works only in power-control mode, not in gain-control mode as in the simulation. Open-loop measurements confirm the agreement between amplifier output power and amplifier gain in our experimental conditions. Our detection setup consists in a photodiode with a bandwidth of 3.5 GHz at -3 dB. The signal is monitored with a 1 GHz-bandwidth oscilloscope and a 6 GHz-bandwidth electrical spectrum analyzer.

3. Opto-RF Generation and Waveforms Characterization

In the following, we challenge (6) against various experimental situations. Namely, we first measure the RF comb expansion versus the YDFA gain parameter, then we observe the nature of the waveforms (i) when the delay time (e.g., the RF phase) is discretely modified, or (ii) when the RF driving frequency is scanned. In order to compute the power time series, we use all the experimentally measured parameters given above. γ is therefore the only fitting parameter.

3.1 RF Up-Conversion

To demonstrate the ability of generating high-order harmonics, the loop length and shift frequency are fixed, and the fiber YDFA is set to different powers. The loop optical length of the ring cavity is equal to 18.55 m; the frequency of AOFS is set at 200 MHz. The seed laser power is kept at 50 mW.

The influence of the loop net gain on the beat note spectrum is shown in Fig. 2(a)–(f). Fig. 2(a)–(c) report the simulation results with amplifier gains of 1, 2.5 and 3.5, respectively. When $G = 1$, the highest order harmonics of the beat note is 10th, which corresponds to 2 GHz. As G increases up to 3.5, the 20th harmonics of beat signal appears. In order to verify experimentally the simulation

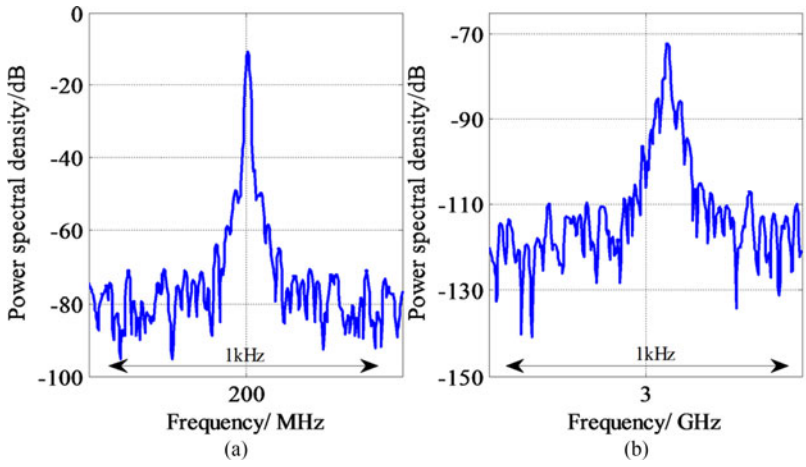

Fig. 3. Beat harmonics spectra (span 1 kHz, RBW 10 Hz). (a) 1st harmonics at 200 MHz; (b) 15th harmonics at 3 GHz. 3-dB linewidths are 10 Hz instrument-limited in both cases.

results, measurements are performed with different amplifier powers. We set the amplifier power to 15 mW, 20 mW, and 25 mW, respectively As shown in Fig. 2(d)–(f), the highest order of beat note harmonics increases from 15th (3 GHz) to 19th (3.8 GHz) when the amplifier output power increases from 15 mW to 25 mW. Note that this spectrum is limited by the photodiode bandwidth. The experimental results are in good agreement with the simulations.

In order to evaluate the spectral purity of the beat notes generated by this method, we compare the 1st and the 15th harmonics (3 GHz) on a high-resolution mode. As shown in Fig. 3, the linewidth (FWHM) of the 15th harmonics (3 GHz) is as narrow as of 1st harmonics (200 MHz), i.e., limited by the 10 Hz-resolution bandwidth of the instrument. As expected, the cumulative delay time being far below the coherence time of the laser source, high-order harmonics keep narrow linewidths. This point is of interest for Doppler measurements that will be described in Section 4.

3.2 Influence of the Loop Length

The ring interferometer loop length determines the phase factor of each RF harmonics, which eventually leads to different interference waveforms in the time domain. In order to investigate this property, we choose $f_{AO} = 200$ MHz and G = 3.5 (corresponding to an amplifier output power of 25 mW), and we use extra fibers of different lengths to modify the loop length by steps of 15 cm. For example, we show the results obtained for optical lengths $n_g L = 18.55$ m, 18.70 m, 18.85 m, and 19.00 m, respectively.

The simulation and experiment waveform of beat note are shown in Fig. 4 on a 15 ns time span. In the simulation (in red on the Figure), we find the period to be 5 ns, as expected from the fundamental f_{AO}. Then, depending on the loop length, various waveforms are observed. It is worthwhile to note that $n_g L = 19.00$ m corresponds to an integer multiple of the beat wavelength (200 MHz), leading to an inverted pulse (or dark pulse) waveform. Experimentally, we add 15 cm long pieces of fiber, and observe the corresponding waveforms as depicted in Fig. 4(e)–(h). A very good agreement is obtained with the simulations. The smoother shapes obtained experimentally are due to the oscilloscope 1 GHz-bandwidth that is much lower than the highest harmonics of the beat note.

3.3 Influence of the Shifting Frequency

Conversely, we now fix the loop length and we study the role of the shifting frequency f_{AO}. In contrast with the preceding method, the RF phase is here continuously tunable. The loop length is set at 18.55 m and the output amplifier power at 25 mW, corresponding to $G = 3.5$ in the simulation.

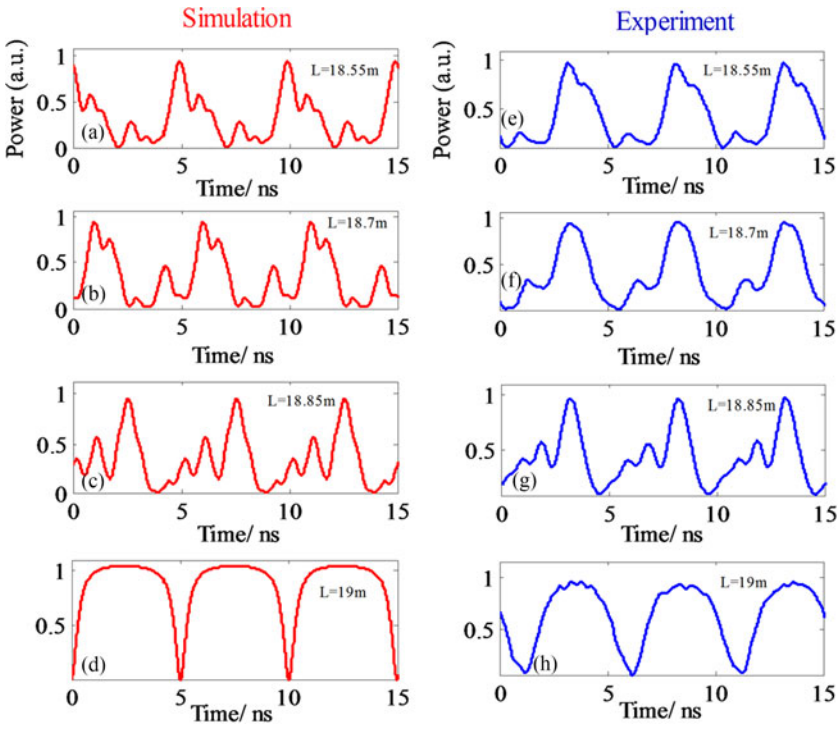

Fig. 4. Influence of the loop length on the waveform. (a)–(d) Simulations (red lines), and (e)–(h) corresponding experimental traces (blue lines).

Simulation and experiment waveforms are shown in Fig. 5. As typical examples, we choose to depict pulse-like, square-shaped and triangle-shaped waveforms that are obtained for 201 MHz, 199.5 MHz and 203.4 MHz, respectively. Again, we find a very good agreement between simulated and experimental waveforms. It shows that a combination of discrete and continuous tuning of the RF phase, either by changing the fiber loop length or the acousto-optic driving frequency, permits to generate a wide variety of waveforms.

4. Application to Doppler Velocimetry

RF-modulated laser based on the frequency-shifting amplifying loop has the ability of generating high-order harmonics and the high-order harmonics can keep high spectral purity as the fundamental frequency. Here we focus on a direct application of this source: a velocity measurement with different order harmonics. The velocity experiment is described in Fig. 6. The components of the transmitter are the ones defined in Fig. 2. The emitted wave from the frequency-shifting amplifying loop is directed through a fiber coupler with a splitting ratio of 1:99. The 99% output is connected to a fiber circulator, and the other one (1%) is directly detected by photodetector PD2 (5 GHz bandwidth) and used as a monitor signal. The light beam emitted by the circulator is collimated by a 10-cm-diameter lens and transmitted to the moving target. The target consists of a 10-cm-diameter retro-reflective prism mounted on a 2-m long electric translation stage. The target moves toward and away from the laser in one cycle at a speed v adjustable from 0.1 ms^{-1} to 0.8 ms^{-1}.

To measure the Doppler shift f_D, the backscattered laser is collected and detected by another high-speed photodetector PD1 (3.5 GHz bandwidth). The signal processing is thus simply a Fourier transform, with a resolution bandwidth (RBW) here equal to 1 Hz. Because the movement of the electric translation stage is a back-and-forth motion, we measure two Doppler shifts with opposite direction and the difference is simply $f_D = \frac{4v}{c}(nf_{AO})$, as shown in Fig. 7. A target velocity $v = 0.8\,ms^{-1}$ and a fundamental frequency 200 MHz will theoretically lead to a frequency shift of 2.13 Hz. Of

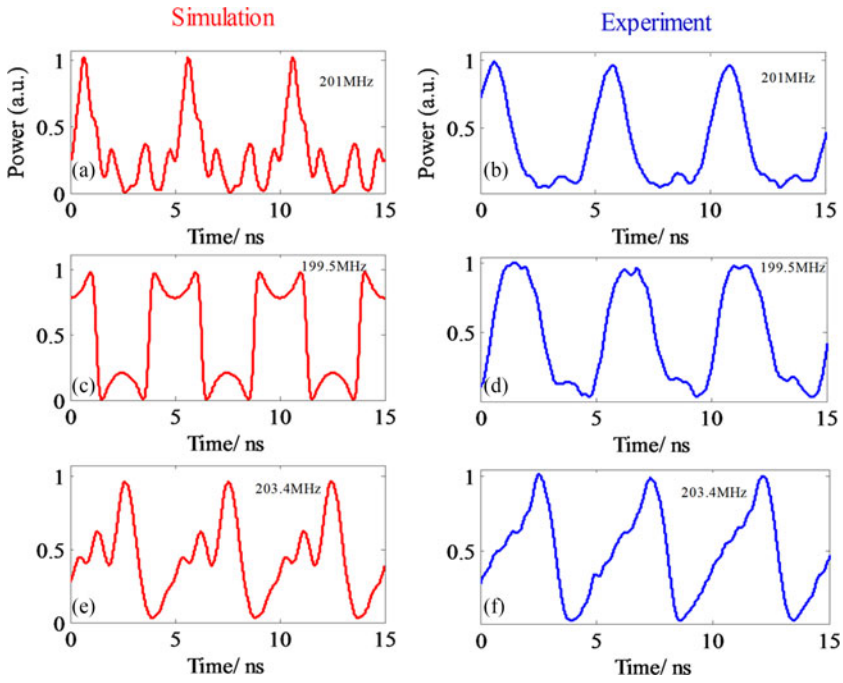

Fig. 5. Influence of the modulation frequency. (blue line: experiment; red line: simulation) (a) Simulated and (b) Experimental waveform with modulation frequency 201 MHz; (c) Simulated and (d) Experimental waveform with modulation frequency 199.5 MHz; (e) Experimental and (f) Simulated waveform with modulation frequency 203.4 MHz

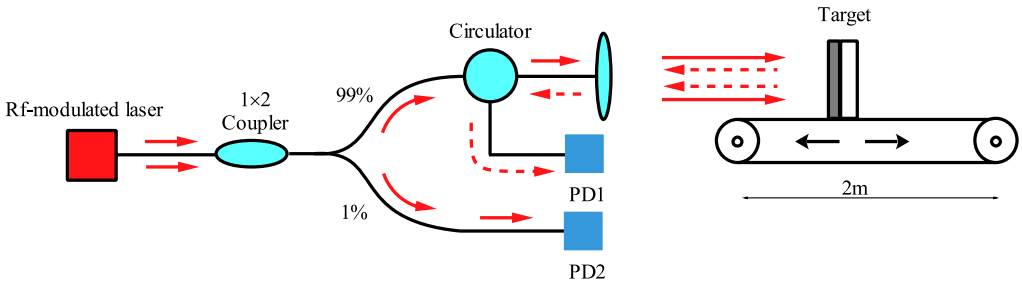

Fig. 6. Schematic of the experiment setup for measuring the linear velocity of a back-and-forth moving target.

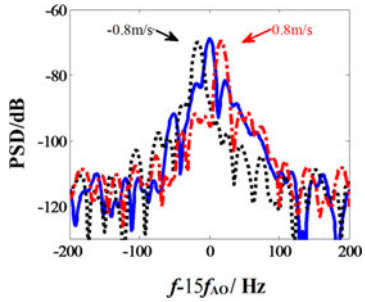

Fig. 7. Doppler-shift measurement by spectral analysis of the backscattered beam Span: 1 kHz. RBW: 1 Hz. The PSD is shown around 3 GHz (harmonics order $n = 15$). Left peak (black): v $= -0.8$ ms^{-1}. Central peak (blue): v $= 0$ ms^{-1}. Right peak (red): v $= +0.8$ ms^{-1}.

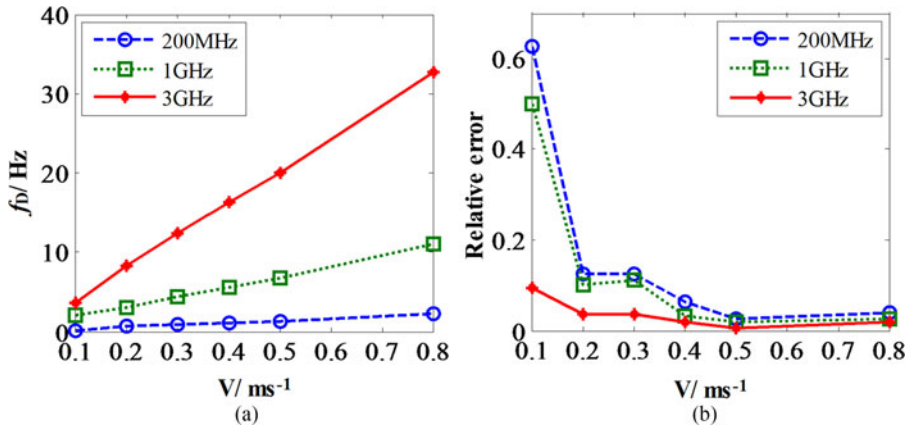

Fig. 8. (a) Doppler shifts and (b) relative velocity error for different harmonics orders. The measured RF lines are 200 MHz (blue), 1 GHz (green), and 3 GHz (red), respectively.

course the frequency shift evolves with the velocity or the harmonics order. For example, when the harmonics order is $n = 15$ (corresponding to a 3 GHz RF modulation), the frequency shift should be 32 Hz, which could alleviate the effects of ultra-low Doppler frequency shift. Fig. 8(a) plots the Doppler shifts for different values of velocity and harmonics orders. We find (i) a good linear dependency of the frequency shift versus motor velocity, and (ii) the expected n-fold enhancement of the slopes.

For such velocity detection based on the RF-modulated laser, the velocity resolution is determined by the bandwidth of the Doppler-shifted signal. Since it was shown above (see Fig. 3) that the 15th harmonics is as narrow as the fundamental frequency (i.e., limited by our measurement detection chain), then the resolution of the velocity measurement can be improved n times compared with fundamental frequency. We compare in Fig. 8(b) the relative error in our measurement system for different harmonics. At low velocities, the digital sampling limits the resolution, while at higher velocities the resolution is expected to be weakened by the mechanical system itself. From statistical averaging of the measured frequencies, we plot the $\Delta v/v$ relative velocity error. As shown in Fig. 8(b), the absolute velocity error is reduced as the harmonics order increases from $n = 1$ (200 MHz) to $n = 15$ (3 GHz) at all velocities. This measurement confirms that RF up-conversion permits to significantly improve the experimental accuracy at low velocities.

5. Conclusion

The ring interferometer containing an acousto-optic frequency shifter and an amplifier has been shown here to provide RF frequency comb extension. Starting with a 200 MHz acoustic frequency, an instrument-limited 10 Hz-linewidth RF at 3 GHz is demonstrated. In the time domain, we show that the waveform is highly dependent on the RF phase that is governed by the loop length, as well as the acoustic frequency. All the experimental results obtained in a full-fibered experiment at 1064 nm are in good agreement with a simple model. It also provides a simple means to generate high-frequency modulated waves that can face the challenge of ultra-low velocity Doppler frequency shifts. Indeed, we have demonstrated a velocity measurement in laboratory conditions and shown the sensitivity and accuracy improvement obtained with the higher harmonics.

This method also offers a programmable scheme that can be easily integrated. An additional frequency-doubling stage could yield a source at 532 nm for underwater communications. Extension of the scheme to the 1.5 μm telecommunication window is straightforward, in order to target radio-over-fiber applications [17]. Frequency shifters such as dual-drive Mach-Zehnder modulators would allow to reach waveform generation at higher repetition rates, e.g., 10 GHz [21].

References

[1] B. Cochenour, L. Mullen, and J. Muth, "Modulated pulse laser with pseudorandom coding capabilities for underwater ranging, detection, and imaging," *Appl. Opt.*, vol. 50, no. 33, pp. 6168–6178, 2011.

[2] G. Pillet, L. Morvan, D. Dolfi, and J.-P. Huignard, "Wideband dual-frequency lidar-radar for simultaneous velocity and high-resolution range profile measurements," in *Proc. SPIE*, 2009, vol. 7323, Art. no. 73230Z.

[3] R. Diaz, S. C. Chan, and J. M. Liu, "Lidar detection using a dual frequency source," *Opt. Lett.*, vol. 31, no. 24, pp. 3600–3602, 2006.

[4] M. Vallet *et al.*, "Lidar-radar velocimetry using a pulse-to-pulse coherent RF-modulated Q-switched laser," *Appl. Opt.*, vol. 52, no. 22, pp. 5402–5410, 2013.

[5] Z. Zheng *et al.*, "Phase noise reduction by using dual-frequency laser in coherent detection," *Opt. Laser Technol.*, vol. 80, pp. 169–175, 2016.

[6] C. H. Cheng, C. W. Lee, T. W. Lin, and F. Y. Lin, "Dual-frequency laser Doppler velocimeter for speckle noise reduction and coherence enhancement," *Opt. Exp.*, vol. 20, no. 18, pp. 20255–20265, 2012.

[7] Z. Zheng *et al.*, "Influence of speckle effect on Doppler velocity measurement," *Opt. Laser Technol.*, vol. 80, pp. 22–27, 2016.

[8] H. Zhang, M. Brunel, M. Romanelli, and M. Vallet, "Green pulsed lidar-radar emitter based on a multipass frequency-shifting external cavity, "*Appl. Opt.*, vol. 55, no. 10, pp. 2467–2473, 2016.

[9] Y. Bai, D. Ren, W. Zhao, Y. Qu, L. Qian, and Z. Chen, "Heterodyne Doppler velocity measurement of moving targets by mode-locked pulse laser," *Opt. Exp.*, vol. 20, no. 2, pp. 764–768, 2012.

[10] P. Ghelfi *et al.*, "A fully photonics-based coherent radar system," *Nature*, vol. 507, pp. 341–345, 2014.

[11] H. Tsuchida, "Simple technique for improving the resolution of the delayed self-heterodyne method," *Opt. Lett.*, vol. 15, no. 11, 640–642, 1990.

[12] J. W. Dawson, N. Park, and K. J. Vahala, "An improved delayed self-heterodyne interferometer for linewidth measurements," *IEEE Photon. Technol. Lett.*, vol. 4, no. 9, 1063–1065, Sep. 1992.

[13] M. Han and A. Wang, "Analysis of a loss-compensated recirculating delayed self-heterodyne interferometer for laser linewidth measurement," *Appl. Phys. B*, vol. 81, pp. 53–58, 2005.

[14] F. V. Kowalski, S. J. Shattil, and P. D. Halle, "Optical pulse generation with a frequency shifted feedback laser," *Appl. Phys. Lett.*, vol. 53, no. 9, pp. 734–736, 1988.

[15] H. Sabert and E. Brinkmeyer, "Pulse generation in fiber lasers with frequency shifted feedback," *J. Lightw. Technol.*, vol. 12, no. 8, pp. 1360–1368, Aug. 1994.

[16] H. G. de Chatellus, E. Lacot, W. Glastre, O. Jacquin, and O. Hugon, "Theory of talbot lasers," *Phys. Rev. A*, vol. 88, 2013, Art. no. 033828.

[17] A. Kanno *et al.*, "16-Gbaud QPSK radio transmission using optical frequency comb with recirculating frequency shifter for 300-GHz RoF signal," in *Proc. IEEE Microw. Photon. Int. Conf.*, 2012, pp. 298–301.

[18] H. G. de Chatellus, L. R. Cortés, and J. Azaña, "Optical real-time Fourier transformation with kilohertz resolutions," *Optica*, vol. 3, pp. 1–8, 2016.

[19] M. Wan *et al.*, "Rapid, k-space linear wavelength scanning laser source based on recirculating frequency-shifter," *Opt. Exp.*, vol. 24, no. 24, pp. 27614–27621, 2016.

[20] A. Yariv, "Universal relations for coupling of optical power between microresonators and dielectric waveguides," *Electron. Lett.*, vol. 36, no. 4, pp. 321–322, 2000.

[21] B. Dai, Z. Gao, X. Wang, H. Chen, N. Kataoka, and N. Wada, "Generation of versatile waveforms from CW light using a dual-drive Mach-Zehnder modulator and employing chromatic dispersion," *J. Lightw. Technol.*, vol. 31, no. 1, pp. 145–151, Jan. 2013.